Peer-reviewed version available at *Remote Sens.* **2018**, *10*, 1698; doi:10.3390/rs10111698

Article

Fast Atmospheric Correction Method for Hyperspectral Data

Leonid V. Katkovsky [1]*, Anton O. Martinov [1], Volha A. Siliuk [1], Dimitry A. Ivanov[1], and Alexander A. Kokhanovsky [2]

[1] A. N. Sevchenko Research Institute of Applied Physical Problems, Belarus State University, BY-220045, Minsk, Belarus; katkovskyl@bsu.by
[2] VITROCISET, Bratustrasse 7, 64293 Darmstadt, Germany
* Correspondence: katkovskyl@bsu.by; Tel.: +375-17-207-0773

Abstract: Atmospheric correction is a necessary step in processing data recorded by spaceborne sensors for cloudless atmosphere, primarily in the visible and near-IR spectral range. In this paper we present a fast and sufficiently accurate method of atmospheric correction based on the analytical solutions of radiative transfer equation (RTE). The proposed analytical equations can be used to calculate the spectrum of outgoing radiation at the top boundary of the cloudless atmosphere. The solution of the inverse problem for finding unknown parameters of the model is carried out by the method of non-linear least squares (Levenberg-Marquardt algorithm) for an individual selected pixel of the image, taking into account the adjacency effects. Using the found parameters of the atmosphere and the average surface reflectance, and also assuming homogeneity of the atmosphere within a certain area of the hyperspectral image (or within the whole frame), the spectral reflectance at the Earth's surface is calculated for all other pixels. It is essential that the procedure of the numerical simulation using non-linear least squares is based on analytical solution of the direct transfer problem. This enables fast solution of inverse problem in a very short calculation time. Testing of the method has been performed using the synthetic outgoing radiation spectra at the top of atmosphere, obtained from the LibRadTran code. Also we have used the spectra measured by the Hyperion. A comparison with the results of atmospheric correction in module FLAASH of ENVI package has been performed. Finally, to validate data obtained by our method, a comparative analysis with ground-based measurements of Radiometric Calibration Network (RadCalNet) was carried out.

Keywords: satellite sensors; spectral- and hyperspectral imaging; atmospheric model; outgoing radiation; atmospheric correction; spectral radiance; surface reflectance; spectral brightness factor (coefficient).

1. Introduction

The main task of the atmospheric correction is to find a relation between the surface spectral reflectance and the spectral radiance at the top of atmosphere (TOA), measured by satellite sensors. Atmospheric correction methods can be divided into empirical and based on radiative transfer models [1]. The first class of methods is based on the use of *a-priori* information about the object with which one can perform atmospheric correction without detailed radiation transfer modeling. The second class of methods is more accurate, but, in turn, requires more complex and time-consuming calculations.

There are a number of radiative transfer codes for the atmospheric correction: ACORN (Atmospheric CORrection Now) [2], based on MODTRAN-4; ATCOR (ATmospheric CORrection) [3], ERDAS Imagine; ATREM (ATmospheric REMoval), [4]; FLAASH (Fast Line-of-sight Atmospheric Analysis of Spectral Hypercubes) [5], RSI ENVI; HATCH (High-accuracy ATmospheric Correction for Hyperspectral data) [6,7], improved ATREM code; Tafkaa [8], based on ATREM. Most of these codes are designed for the specific satellite imaging systems, a certain spectral range, a set of spectral bands, spectral and spatial resolutions. The disadvantages of many techniques is the use of complex

algorithms of the RTE solution [9] or pre-calculated look-up-tables, followed by interpolation [5], that requires a considerable time, or is unsatisfactory in accuracy. Generally, at the same time, they require a certain *a-priori* data about the parameters of the atmosphere. In [10] a fast method for reconstructing the aerosol optical thickness of the atmosphere is proposed, based on a combination of analytical and numerical solutions for various scattering layers positioned in atmosphere, which can also be successfully used to obtain the reflectance spectra of the underlying surface.

A more detailed description of the existing methods and software is given by Katkovsky [11]. A fast method of atmospheric correction presented in this paper does not require complex calculations and usage of *a-priori* data.

2. Atmospheric model

Our atmospheric model includes the following processes:

- molecular (Rayleigh) scattering,
- aerosol absorption and scattering,
- absorption by water vapor, oxygen and ozone.

The development of the optical model of the atmosphere is a necessary step in solving any inverse problem. Atmospheric models used in atmospheric radiative transfer studies usually account for the latitudinal zones, different seasons and vertical profiles of the scattering layers [12]. However, our analysis of the numerous spectral radiance calculations for various solar/observation angles and atmospheric models has shown that the spectrum of outgoing radiation [13] is weakly dependent on the vertical stratification of the atmosphere. A similar conclusion has been reached in [10], in relation to the stratification of the lower layer of the troposphere. Essential parameters used by us for the calculation of the spectrum of outgoing radiation are:

- measurement geometry,
- the spectral land surface reflectance,
- vertical optical thickness of molecular scattering,
- aerosol optical thickness,
- scattering phase function parameter (average cosine of scattering angle),
- single scattering albedo,
- integrated content of water vapor (in the column of the atmosphere), oxygen, and ozone.

The spectra of outgoing radiation (outside the absorption bands of atmospheric gases) are most sensitive to variation of (in descending order of influence) surface reflectance, total vertical optical thickness and the average cosine of the scattering angle.

In particular, we have used the parameters of the optical model of the cloudless atmosphere discussed below.

1) *Vertical optical thickness of the atmosphere* at the wavelength λ (excluding optical thickness for gaseous absorption) is defined as

$$\tau_\lambda = \tau_{\mathbf{sca,m}} + \tau_{\mathbf{sca,a}} + \tau_{\mathbf{abs,a}}, \quad (1)$$

where $\tau_{\mathbf{sca,m}}$ is optical thickness of molecular (Rayleigh) scattering; $\tau_{\mathbf{sca,a}}$ is optical thickness of aerosol scattering; $\tau_{\mathbf{abs,a}}$ is optical thickness of aerosol absorption.

2) *Single scattering albedo* (quantum survival probability) ω_λ is calculated as follows:

$$\omega_\lambda = \left(\tau_{\mathbf{sca,m}} + \tau_{\mathbf{sca,a}}\right) / \left(\tau_{\mathbf{sca,m}} + \tau_{\mathbf{sca,a}} + \tau_{\mathbf{abs,a}}\right). \quad (2)$$

3) *The vertical molecular optical thickness* is determined by the atmospheric model (season and location) [14]

$$\tau_{\mathbf{sca,m}} = F\left(P_s, T_s\right) \lambda^{-(B+C\lambda+D/\lambda)} \frac{T_s}{T_0} \frac{P_0}{P_s}. \tag{3}$$

Constants in Eq. (3) are the following: the pressure P_s and the temperature T_s at the Earth's surface are taken in the selected atmospheric model (for example, Midlatitude Summer); P_0 and T_0 are real values of pressure and temperature, accordingly, at the Earth's surface at the measurement time; constants B, C, D are independent on atmospheric models. We have used six types of the atmospheric models, values of the coefficients for which are given in Table 1.

Table 1. Values of coefficients for calculating the Rayleigh optical thickness of the total atmosphere from Eq.(3)

	Atmospheric model	$\lambda = 0.2 - 0.5\mu m$	$\lambda > 0.5\mu m$	**pressure P_s, mbar at the Earth's surface**	**temperature T_s,K at the Earth's surface**
B	For all models	3.55212	3.99668		
C		1.35579	0.00110298		
D		0.11563	0.0271393		
$F\left(P_s, T_s\right)$	Tropical	0.006525841	0.008680089	1013	300
	Midlatitude Summer	0.006515547	0.008665997	1013	294
	Midlatitude Winter	0.006531896	0.008688402	1018	272.2
	Subarctic Summer	0.006477539	0.008616175	1010	287
	Subarctic Winter	0.006495823	0.008641742	1013	257.1
	1962 US Standard	0.006499595	0.008645261	1013	288.1

The spectral dependence of the aerosol optical thicknesses introduced in the atmospheric model is approximated by the power law function:

$$\tau_{\mathbf{sca,a}} = \tau_{\mathbf{sca,a0}} (\lambda_0/\lambda)^{\beta}, \tag{4}$$

where $\tau_{\mathbf{sca,a0}}$ is the corresponding optical thickness at the reference wavelength λ_0, β is Ångstroem exponent. The value of $\tau_{\mathbf{abs,a}}$ is supposed to be not dependent on the wavelength (it is usually small as compared to $\tau_{\mathbf{sca,a}}$).

4) *The spectral reflectance of the underlying surface* ρ_λ is considered to be Lambertian (isotropic).

5) *The total scattering phase function* is given as the weighted-average function of the Rayleigh $x_m(\gamma)$ and $x_a(\gamma)$ the aerosol scattering phase functions as follows:

$$x(\gamma) = x_m(\gamma)\tau_{\mathbf{sca,m}} / \left(\tau_{\mathbf{sca,m}} + \tau_{\mathbf{sca,a}}\right) + x_a(\gamma)\tau_{\mathbf{sca,a}} / \left(\tau_{\mathbf{sca,m}} + \tau_{\mathbf{sca,a}}\right), \tag{5}$$

where aerosol scattering phase function is approximated by Henyey-Greenstein function. In particular, it follows:

$$\begin{aligned} x_m(\gamma) &= \frac{3}{4}(1+\gamma^2) \\ x_a(\gamma) &= \left(1 - g_{\mathbf{a}}^2\right) / \left(1 + g_{\mathbf{a}}^2 - 2g_{\mathbf{a}}\gamma\right)^{3/2} \\ \gamma &= -\mu\mu_0 + \sqrt{(1-\mu^2)(1-\mu_0^2)}\cos\varphi, \end{aligned} \tag{6}$$

with an average cosine of scattering angle, $g_{\mathbf{a}}$, which is assumed to be independent on the wavelength. However, by means of Eq. 5, the spectral dependence of the total scattering phase

function on the wavelength is introduced. In Eq. 6, γ is cosine of the scattering angle, the Sun zenith angle $\Theta_0 = \arccos \mu_0$, μ is cosine of the zenith angle of observation Θ, φ is azimuth angle of radiation propagation direction with respect to the solar vertical plane. The scattering angle γ (and $x(\gamma)$) is used later only in the term for atmospheric haze radiation. According to [10], the choice of the scattering phase function is not important in determining the surface reflectance, because the equation includes the product of aerosol optical thickness and the phase function, each of which may be incorrectly defined, but the product and the value of the surface reflectance is correctly determined.

Accounting for the absorption bands of the major gaseous components of the atmosphere (water vapor, ozone and oxygen) is performed by filter method, that is, we use the general expression for spectral reflectance at TOA recorded excluding gas absorption components, multiplied by the transmissions of the three gas each components:

$$T_g(\lambda) = T_{\mathbf{H_2O}\lambda} T_{\mathbf{O}_2\lambda} T_{\mathbf{O}_3\lambda}. \tag{7}$$

To account for the transmission in the bands of absorption of these gases atmospheric transmissions were calculated for standard absorbing mass values each of these components with a spectral resolution of 2 nm, at the zenith Sun's location, nadir viewing, twice the radiation passage (up- and downwelling) and average surface reflectance 0.2, as shown on Fig.1 in [11]. The standard conditions used to calculate the transmissions correspond to the following values of various parameters:

- standard surface temperature 293K;
- standard surface pressure 101.3kPa;
- standard total integrated precipitable water: 4.20g/cm^2;
- standard integrated ozone amount 0.330$atm \cdot cm$.

For transmission with the absorbing mass, which differs from the standard for other Sun's and observation angles it is necessary to use the following expressions are used:

$$T_{\mathbf{H_2O}\lambda} = \left(T^0_{\mathbf{H_2O}\lambda}\right)^{m_1}, \quad T_{\mathbf{O}_2\lambda} = \left(T^0_{\mathbf{O}_2\lambda}\right)^{m_2}, \quad T_{\mathbf{O}_3\lambda} = \left(T^0_{\mathbf{O}_3\lambda}\right)^{m_3}, \tag{8}$$

where $T^0_{\mathbf{H_2O}\lambda}, T^0_{\mathbf{O}_2\lambda}, T^0_{\mathbf{O}_3\lambda}$ are standard transmission functions of respective gaseous components for the conditions given above.

The following assumptions were used for the concentration profiles of atmospheric gases:

- The fixed oxygen content is assumed, so the parameters m_2 depend only on the air mass.
- In contrast, due to considerable variability, the transmission function of water vapor depends on the unknown concentration. The parameter m_1 is adjustable, including both the concentration of water vapor and the effective path of radiation (effective air mass).
- Although variations in the ozone concentration are usually minor, the public datasets of the European Center for Medium-Range Weather Forecasts (ECMWF) to estimate the actual ozone concentration in the selected area were used.

Thus, in order to reduce unknown parameters in the solution of the inverse problem, the parameters m_2, m_3 are assumed to be known (calculated) when solving the first stage of the inverse problem. In the next step, aimed at finding the surface reflectance of each pixel, parameters are re-estimated.

It should be noted that the use of a relatively simple model of the aerosol component of the atmosphere (see. Eqs. (4)-(6)) also agrees with the conclusions of the paper [10] that, on the one hand, the spectra of outgoing radiation on TOA in the range 400-900 nm do not contain sufficient information to uniquely select aerosol type (four unknown parameters are entered for describing aerosol ($\tau_{\mathbf{sca,a0}}$,

Peer-reviewed version available at Remote Sens. 2018, 10, 1698; doi:10.3390/rs10111698

$\tau_{\mathbf{abs,a}}$, β, $g_{\mathbf{a}}$), but, on the other hand, retrieved spectra of surface reflectance are sufficiently stable with respect to the aerosol model of the atmosphere. This means that the spectrum of outgoing radiation depends on the aerosol model but this dependence is not so strong as on the parameters mentioned above.

3. Approximate analytical equation for spectral radiance at TOA

We use for the at-sensor (satellite) spectral reflectance the following expression:

$$R_\lambda(\mu,\mu_0,\varphi) = \left[R_{\mathbf{atm}\lambda}(\mu,\mu_0,\varphi) + E_\lambda(\mu_0,\rho_{e\lambda})\left(T_\lambda^{\mathbf{dir}}(\mu)\rho_\lambda + \rho_{e\lambda}T_\lambda^{\mathbf{dif}}(\mu)\right)\right]T_{g\lambda}, \tag{9}$$

where $R_{\mathbf{atm}\lambda}(\mu,\mu_0,\varphi) = B_{\mathbf{atm}\lambda}(\mu,\mu_0,\varphi)/\mu_0 S_\lambda$, $B_{\mathbf{atm}\lambda}(\mu,\mu_0,\varphi)$ is spectral radiance of atmospheric haze, S_λ solar brightness constant, $R_{\mathbf{atm}\lambda}(\mu,\mu_0,\varphi)$ is the spectral atmospheric reflectance of haze (corresponds to zero surface reflectance), $\rho_{e\lambda}$ is the average surface reflectance around the current pixel with the reflectance ρ_λ, $E_\lambda(\mu_0,\rho_{e\lambda})$ is the spectral illuminance of the Earth's surface, normalized to that on TOA one, $E_{0\lambda} = \pi S_\lambda \mu_0$, depending on the average surface reflectance $\rho_{e\lambda}$ and zenith solar angle; $T_\lambda^{\mathbf{dir}}(\mu)$, $T_\lambda^{\mathbf{dif}}(\mu)$ are direct and diffuse atmospheric transmission, respectively, from the surface to satellites sensor excluding gas transmission (which is included to the term $T_{g\lambda}$). Total transmission (without gaseous absorbing bands) is the sum of direct and diffuse transmissions:

$$T_\lambda(\mu) = T_\lambda^{\mathbf{dir}}(\mu) + T_\lambda^{\mathbf{dif}}(\mu) = \exp\left(-\tau_\lambda/\mu\right) + T_\lambda^{\mathbf{dif}}(\mu). \tag{10}$$

It should be noted that Eq. (9) differs in form, but is completely equivalent to the generally written equation given in [15], which, in addition to the quantities described above, also includes the downwelling transmission (from TOA to the surface) $T_\lambda^{\downarrow}(\mu)$ and spherical albedo of the atmosphere $s(\lambda)$. We obtain an expression for spectral radiance in this form by substituting in (9) the expression for normalized on the Earth's surface illuminance $E_{0\lambda} = \pi S_\lambda \mu_0$, (see in [16] and [17]):

$$E_\lambda(\mu_0,\rho_{e\lambda}) = \frac{T^{\downarrow}(\lambda)}{1 - s(\lambda)\rho_{e\lambda}}. \tag{11}$$

The basis of analytical approximation for the outgoing radiation (9) consists of expressions for three functions: spectral illuminance $E_\lambda(\mu_0,\rho_{e\lambda})$, total transmission of the atmosphere $T_\lambda(\mu)$ and the spectral reflectance of atmospheric haze $R_{\mathbf{atm}\lambda}(\mu,\mu_0,\varphi)$. The approximation error for each of these functions and Eq. (9) as a whole does not exceed $3-5\%$.

We propose the following approximation for the illuminance (9) with some modification of the Eddington approximation [18,19]:

$$E_\lambda(\mu_0,\rho_\lambda) = \omega_\lambda E_{\mathbf{Ed}\lambda}(\mu_0,\rho_\lambda) + (1-\omega_\lambda)\pi S_\lambda \mu_0 \exp\left(-\tau_\lambda/\mu_0\right) \tag{12}$$

$$E_{\mathbf{Ed}\lambda}(\mu_0,\rho_\lambda) = \frac{4}{4 + 3(1-g_\lambda)(1-\rho_\lambda)\tau_\lambda}\left[\left(\frac{1}{2} + \frac{3}{4}\mu_0\right) + \left(\frac{1}{2} - \frac{3}{4}\mu_0\right)\exp\left(-\frac{\tau_\lambda}{\mu_0}\right)\right]. \tag{13}$$

The average cosine of the scattering angle in Eq. (13) must be calculated in accordance with the definition of the total phase function of the elementary volume (5). Since an average cosine of the scattering angle for molecular one is zero, it follows:

$$g_\lambda = g_{\mathbf{a}}\tau_{\mathbf{sca,a}} / \left(\tau_{\mathbf{sca,m}} + \tau_{\mathbf{sca,a}}\right). \tag{14}$$

The error of approximation Eqs.(12-13) to calculate solar radiation fluxes (illuminance) is 1 - 2% [18], which was also confirmed by the comparisons we carried out with precise calculations using COART program and Eqs.(10)-(11) in the spectral range 0.4-1.1 μm [11].

Preprints (www.preprints.org) | NOT PEER-REVIEWED | Posted: 23 October 2018 doi:10.20944/preprints201809.0119.v3

Peer-reviewed version available at Remote Sens. 2018, 10, 1698; doi:10.3390/rs10111698

For a total transmittance function (excluding absorption gaseous bands) $T_\lambda(\mu)$, an analytic approximation from [20] was used. This approximation is obtained for the values of parameters $0 < g_\lambda < 0.9; \quad 0.2 < \mu < 1.0; \quad 0 < \tau_\lambda < 2$ with a maximum error of about 8% for the $g_\lambda \in [0-0.9], \quad \tau \in [0-2], \quad \mu \in [0.2-1.0]$, and an error of less than 4% for $\tau \leq 1.6, g_\lambda \leq 0.8$ and $\mu \in [0.2-1.0]$.

The advantage of this approximation of the function for total atmospheric upwelling transmittance $T_\lambda(\mu)$ is a sufficiently high accuracy. Moreover, it does not contain new unknown parameters and depends only on total vertical optical thickness of the atmosphere τ_λ, the cosine of the observation angle μ and the average cosine of the scattering angle g_λ.

For the calculation of the spectral reflectance of atmospheric haze $R_{\mathbf{atm}\lambda}(\mu, \mu_0, \varphi)$ in Eq. (9) the following approximation equation was proposed:

$$\begin{aligned} R_{\mathbf{atm}\lambda}(\mu, \mu_0, \varphi) &= R^S_{\mathbf{atm}\lambda}(\mu, \mu_0, \varphi)\,[1 + q(\omega_\lambda \tau_\lambda)^p], \quad p = 1.25 \\ R^S_{\mathbf{atm}\lambda}(\mu, \mu_0, \varphi) &= \frac{\omega_\lambda}{4} \frac{x(\gamma)}{\mu + \mu_0} \left\{ 1 - \exp\left[-\tau_\lambda \left(\frac{1}{\mu_0} + \frac{1}{\mu} \right) \right] \right\}, \end{aligned} \tag{15}$$

in which the contribution of multiple scattering to the radiation of atmospheric haze is taken into account in the form of a quasi-linear amendment to the atmospheric haze reflectance in the single scattering approximation, $R^S_{\mathbf{atm}\lambda}$. Approximation similar to Eq.(15) have been proposed and investigated in [21]. We are using this approximation only for atmospheric haze contributions (for the case of $\rho_\lambda = 0$), where the constant q is unknown adjustable model parameter. We include to the list of unknown values of the inverse problem. Accounting for the contribution of atmospheric haze in a single scattering approach, as the calculations showed, is not satisfactory, even for very clear atmosphere, while the representation (15) provides a sufficiently high accuracy [11].

The set of equations (9), (12) - (15) together with the formulas for the total transmission [20], gives an analytic representation of the spectrum of outgoing radiation, depending on the following seven parameters of the atmospheric optical model and surface:

$$\tau_{\mathbf{abs,a}}, \quad \tau_{\mathbf{sca,a0}}, \quad \beta, \quad g_{\mathbf{a}}, \quad q, \quad \rho_\lambda, \quad m. \tag{16}$$

Note that we put here the index λ for reflectance ρ_λ, emphasizing its dependence on the wavelength. Minimizing the variation of the objective function (9) with respect to the measured value, only spectral independent parameters can be found. Therefore, in the first stage of the algorithm for finding the parameters of the atmosphere, one-parameter function ρ_λ is introduced.

The test results of analytical approximation of spectral reflectance (9), (12) - (15) are given in [11]. The maximum error of the analytic representation in the spectral range of 0.4 - 0.65 microns is less than 4% and it can reach 10% in the range 0.35 - 1.1 microns. However, errors greater than 4% are only observed in the absorption bands of gases, in particular water vapor, suggesting the need for more accurate account for profiles of gaseous components of atmosphere.

We found that even better accuracy can be achieved if instead of one parameter m_1, we use two parameters for the water vapor content (m_{11} and m_{12}): one in the term for the reflection by the haze and other one for the surface. Finally, Eq.(9) could be rewritten (to shorten the reference, hereinafter everywhere we have omitted angular variables):

$$R_\lambda = \left[R_{\mathbf{atm}\lambda}(T_{\mathbf{H_2O}\lambda})^{m_{11}} + E_\lambda(\rho_{e\lambda})(T^{\mathbf{dir}}_\lambda \rho_\lambda + \rho_{e\lambda} T^{\mathbf{dif}}_\lambda)(T_{\mathbf{H_2O}\lambda})^{m_{12}} \right] T^{m_2}_{\mathbf{O_2}\lambda} T^{m_3}_{\mathbf{O_3}\lambda}. \tag{17}$$

4. Atmospheric correction of hyperspectral imagery

The input data for the algorithm are: the reflection spectra of the hyperspectral image R_λ; the geometric parameters (the Sun's zenith angle θ_0, determined by the geographical coordinates and the acquiring time, the recording zenith angle θ (Earth-sensor direction), the azimuth angle ϕ), the TOA

Preprints (www.preprints.org) | NOT PEER-REVIEWED | Posted: 23 October 2018 doi:10.20944/preprints201809.0119.v3

Peer-reviewed version available at Remote Sens. 2018, 10, 1698; doi:10.3390/rs10111698

Sun's brightness function $S_\lambda[W/m^2/\mu m]$, the spectral transmitting functions of oxygen $T_{\mathbf{O}_2\lambda}$, ozone $T_{\mathbf{O}_3\lambda}$, and water vapor $T_{\mathbf{H}_2\mathbf{O}\lambda}$ (dimensionless).

The algorithm of atmospheric correction see (fig. 1) consists of the following basic steps:

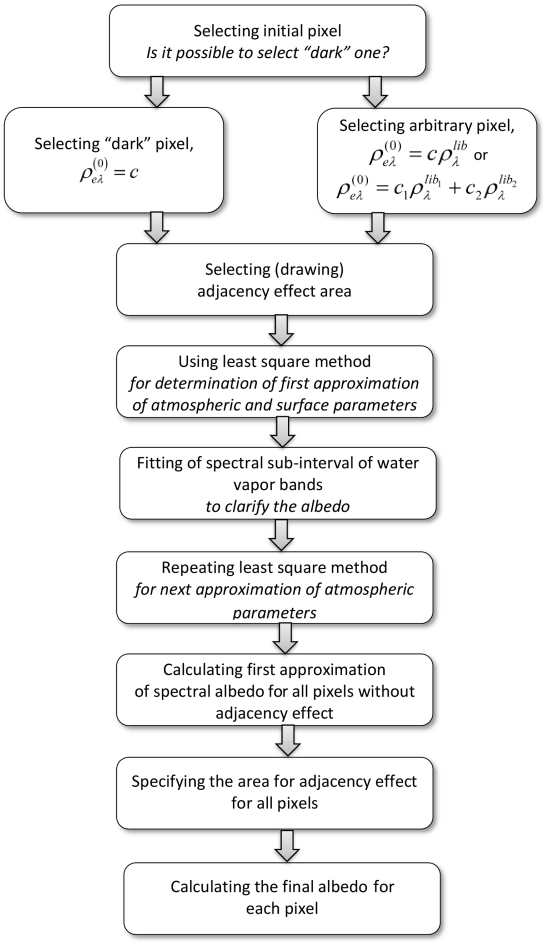

Figure 1. Pipeline of atmospheric correction of hyperspectral image data

1. **The selection of original pixel and area in the image under study for which the atmospheric parameters are determined.**
   (a) We choose a "dark" pixel, if possible, on the hyperspectral image (low reflectance value, it is important to note that it is "dark" in the "blue-green" part of the spectrum, where there is the largest contribution of atmospheric haze). The user has the option of selecting a "dark pixel" either interactively or automatically based on a high correlation of a hyperspectral pixel with the library of various objects such as water, dark soil, asphalt, coniferous forest, etc.
   (b) In case of absent suitable "dark pixel" in the image, a pixel with an approximately identifiable underlying surface (for example: vegetation, water, soil, sand, etc., or a mixture thereof) is selected, which is determined visually from RGB image.

2. **Setup of the initial (zero) algorithm's iteration for the reflectance of the selected pixel.**
   (a) In case of a dark pixel surface (step 1a), we use

$$\rho_\lambda = \rho_\lambda^{(0)} = c, \tag{18}$$

in Eq. (17). Since in this case the contribution of atmospheric haze to the detected signal exceeds the contribution of the reflected radiation from the surface (low reflectance value), then the spectral dependence of ρ_λ can be neglected. Therefore the reflectance can be assumed constant over the spectrum.

(b) In case of a homogeneous pixel (step 1b) ("pure" - vegetation, water, soil, sand, etc), we assume that the spectral surface reflectance function $\rho_\lambda^{(0)}$ of the selected pixel can be presented in the form

$$\rho_\lambda = \rho_\lambda^{(0)} = c\rho_\lambda^{lib}, \tag{19}$$

where c is the unknown weighted positive parameter, ρ_λ^{lib} is the spectral surface reflectance library function of the identified surface type of the selected pixel.

If the selected surface for the pixel is an inhomogeneous (consisting of a mixture of several types of surfaces) one, then the reflectance is assumed to be a linear combination of two dominant surface types with unknown parameter c (which here can vary in the range [0, 1]):

$$\rho_\lambda = \rho_\lambda^{(0)} = c\rho_\lambda^{lib_1} + (c)\,\rho_\lambda^{lib_2}, \tag{20}$$

where $\rho_\lambda^{lib_i}$ is the spectral surface reflectance library. By selecting a pixel over land, it is recommended to choose a linear combination of typical surface reflectance of vegetation and bare soil ([10]).

3. **The choice of the neighborhood around the selected pixel (as an arbitrary polygon).**

   The neighborhood should be (if possible) of the same type (with close reflectance values to the selected source pixel) as the selected pixel itself. The given zero-th order surface reflectance functions for the original pixel are considered as such for the whole selected neighborhood, i.e. are given by one of the formulas (18) - (20).

   The neighborhood area selected here is used to account for an adjacency effect in a non-traditional way: firstly, the initial iteration for atmospheric parameters is made with the average reflection signal via selected area around original (central) pixel, and then the new atmospheric parameters and reflectance of the original (central) pixel are found.

4. **Finding the first iteration of the optical atmospheric parameters and average reflectance of the neighborhood area.**

   We consider for this case $\rho_\lambda = \rho_{e\lambda} = \rho_\lambda^{(0)}$ in (17), where in accordance with the choice of the original pixel, $\rho_\lambda^{(0)}$ is determined by one of the formulas (18) - (20), and one can write (17) in the form

$$\overline{R}_\lambda = \left[R_{\mathbf{atm}\lambda}(T_{\mathbf{H_2O}\lambda})^{m_{11}} + \rho_{e\lambda}^{(0)} E_\lambda(\rho_{e\lambda}^{(0)}) \left(T_\lambda^{\mathbf{dir}} + T_\lambda^{\mathbf{dif}}\right) (T_{\mathbf{H_2O}\lambda})^{m_{12}}\right] T_{\mathbf{O}_2\lambda}^{m_2} T_{\mathbf{O}_3\lambda}^{m_3}. \tag{21}$$

   Here $\overline{R}_\lambda$ is the average spectral reflectance of the hyperspectral image around the original pixel in the user-selected area (neighborhood, step 2). The next step is non-linear fit of the average spectral reflectance of selected area $\overline{R}_\lambda$ by given analytical formula (right-hand side of Eq. 21) with the non-linear least squares Levenberg–Marquardt (LM) algorithm finding a set of unknown optical parameters of the atmosphere (see 16) and average surface reflectance: $\tau_{\mathbf{abs,a}}, \tau_{\mathbf{sca,a0}}, \beta, g_{\mathbf{a}}, q, m_{11}, m_{12}, c_i$. In (16), the water vapor exponent m_1 is replaced by two ones, m_{11} and m_{12} , in accordance with (17), and instead of ρ_λ the weighted parameter c stands here

for the mean reflectance of the chosen neighborhood (from (18) or (20)).

5. **Additional smoothing of the spectral curve ρ_λ of the current pixel in the water absorption spectral bands by re-fitting, where we vary just m_{11} and m_{12}, corresponding to the water vapor.**

6. **Refinement (next iteration).**

   The atmospheric parameters $\tau_{\mathbf{abs,a}}, \tau_{\mathbf{sca,a0}}, \beta, g_\mathbf{a}, q, m_{11}, m_{12}$ and reflectance of the original (central) pixel $\rho_\lambda^{(1)}$, which may differ from the neighborhood reflectance and which determined by one of equation (18) - (20) with a new unknown value of the parameter $c = c_1$ are found. In this case, reflectance of the neighborhood pixels remains the same as in the previous iteration (step 4).

   The (LM) non-linear least squares method is re-started using the following equation, which takes into account an adjacency effect (instead of (21)):

$$R_\lambda = \left[R_{\mathbf{atm}\lambda}(T_{\mathbf{H_2O}\lambda})^{m_{11}} + E_\lambda(\rho_{e\lambda}^{(0)})\left(T_\lambda^{\mathbf{dir}}\rho_\lambda^{(1)} + \rho_{e\lambda}^{(0)}T_\lambda^{\mathbf{dif}}\right)(T_{\mathbf{H_2O}\lambda})^{m_{12}}\right] T_{\mathbf{O_2}\lambda}^{m_2} T_{\mathbf{O_3}\lambda}^{m_3}. \quad (22)$$

   Therefore, the fitting of measured reflection spectrum of the original pixel R_λ is performed by the objective function (22).

7. **Application of smoothing filter to the current pixel by re-fitting using exponents m_2 and m_3.**

8. **Calculation of the first approximation for the surface reflectance ρ_λ.**

   The surface reflectance is found for all other pixels of the hyperspectral image without the adjacency effect from the following quadratic equation (it is obtained by solving the equation (17) for the variable ρ_λ with putting there $\rho_{e\lambda} = \rho_\lambda$ and taking into account the expressions (12,13) for $E_\lambda(\rho_\lambda)$). Atmospheric parameters, which found in step 6 are substituted into Eq. (17) (the atmosphere is assumed horizontally homogeneous, identical over all pixels). Then it follows:

$$a_\lambda\rho_\lambda^2 - b_\lambda\rho_\lambda + c_\lambda = 0, \quad (23)$$

   where

$$a_\lambda = 3\tau_\lambda(1-g_\mathbf{a})(1-\omega_\lambda)\exp(-\tau_\lambda/\mu_0), \quad (24)$$

$$b_\lambda = 3\tau_\lambda(1-g_\mathbf{a})R_{1\lambda} + 4\omega_\lambda\left[\left(\frac{1}{2}+\frac{3}{4}\mu_0\right) + \left(\frac{1}{2}-\frac{3}{4}\mu_0\right)\exp\left(-\frac{\tau_\lambda}{\mu_0}\right)\right] +$$
$$+ [4+3\tau_\lambda(1-g_\mathbf{a})](1-\omega_\lambda)\exp(-\tau_\lambda/\mu_0), \quad (25)$$

$$c_\lambda = [4+3\tau_\lambda(1-g_\mathbf{a})]R_{1\lambda}, \quad (26)$$

$$R_{1\lambda} = \left[R_\lambda / \left(T_{\mathbf{O_2}\lambda}^{m_2} T_{\mathbf{O_3}\lambda}^{m_3}\right) - R_{\mathbf{atm}\lambda}(T_{\mathbf{H_2O}\lambda})^{m_1}\right] \cdot \left[T_\lambda(T_{\mathbf{H_2O}\lambda})^{m_2}\right]^{-1}. \quad (27)$$

   Here R_λ is the spectral reflectance of the processed pixel. Atmospheric parameters found above are substituted into Eqs. (24)-(27).

9. **The adjacency effect area specification by pixel-wise.**

   At this step we specify a fixed neighborhood of each pixel and calculate the average reflectance to account for the adjacency effect. In this case, the spectral surface reflectance of pixels from the previous stage is used. The contribution to the total spectral surface reflectance from neighboring

pixels is accounted for with an exponentially decay weight function depending on distance from the central (current) pixel:

$$\overline{\rho_\lambda} = \frac{1}{N}\sum_{i,j} A \exp\left(-\frac{a\sqrt{i^2+j^2}}{d}\right)\rho_{\lambda,i,j}, \tag{28}$$

where i, j are pixel numbers in the neighborhood, d is the half-width of the specified window in pixels, a, A are the distribution parameters, N is the number of neighboring pixels (d is selected using iterations).

10. **The estimation of final reflectance value.**

The surface reflectance is found from the following formula, which follows from Eq. (28):

$$\begin{aligned}\rho_\lambda = &\left[\frac{R_\lambda}{T_{\mathbf{O}_2\lambda}^{m_2} T_{\mathbf{O}_3\lambda}^{m_3}} - R_{\mathbf{atm}}^{\lambda}\left(T_{\mathbf{H_2O}\lambda}\right)^{m_{11}} - \overline{\rho}_\lambda E_\lambda(\overline{\rho}_\lambda) T_\lambda^{\mathbf{dif}}\left(T_{\mathbf{H_2O}\lambda}\right)^{m_{12}}\right] \\ &\cdot\left[E_\lambda(\overline{\rho}_\lambda) T_\lambda^{\mathbf{dir}}\left(T_{\mathbf{H_2O}\lambda}\right)^{m_{12}}\right]^{-1}\end{aligned} \tag{29}$$

where one needs to substitute the following values: the spectral reflectance of the processed (current) pixel R_λ, the average spectral surface reflectance estimated for each current pixel using Eq. (28) (calculated based on step 8) and atmospheric parameters found in step 6.

5. Validation

5.1. Validation using synthetic spectra

The developed method SHARC (Sattelite Hypercube Atmosheric Rapid Correction) was first tested using the spectra of outgoing radiation, obtained by numerical calculation of radiation transfer equation using the well-known open access programming code LibRadTran [22].

The validation using radiative transfer modeling, say, with LibRadTran, is an important part of the atmospheric correction, since it represents the most "clean" task version (without influence some negative factors of real measurements), and therefore, it allows to verify the adequacy and accuracy of the atmospheric model and the analytical expressions used. The purpose of validation of the atmospheric correction method using the numerical calculations of the outgoing radiation spectrum is to check the method of atmospheric correction in the form that most corresponds to the objective function used for the solution of the inverse problem, that is the analytical spectral radiance function. What is this correspondence? A numerical calculation of the spectral radiance is carried out for a separate observation beam (as well as Eq. (17)), i.e. the problem is one-dimensional one. The surface and atmosphere are horizontally uniform, whereas the experimental value of the spectral radiance from satellite sensor is averaged over the finite instantaneous field of view corresponding to a single pixel. In the numerical calculation of spectral radiance, the adjacency effect is not taken into account. It is also omitted in the analytical equations in this validation part (one should use $\rho_{e\lambda} = \rho_\lambda$ in Eq. 17), but it is taken into account for real satellite data (there is a problem of the neighborhood influence selection, e.g., selection of the adjacency effect radius). Furthermore, usually instrumental errors are present while working with satellite imagery, whereas for numerically calculated spectral radiance, such errors are absent.

As shown by numerical calculations, the accuracy of the emission spectrum at the top of atmosphere by analytical equations is very high, which is confirmed by Fig. 2. In Fig. 2 we show two curves of the brightness (instead of the reflection coefficient) at TOA direct problem: obtained by numerical calculation of LibRadTran with the underlying surface "grass" and fitting curve of non-linear least squares LM algorithm with the analytical Eq(21).

Preprints (www.preprints.org) | NOT PEER-REVIEWED | Posted: 23 October 2018 doi:10.20944/preprints201809.0119.v3

Peer-reviewed version available at Remote Sens. 2018, 10, 1698; doi:10.3390/rs10111698

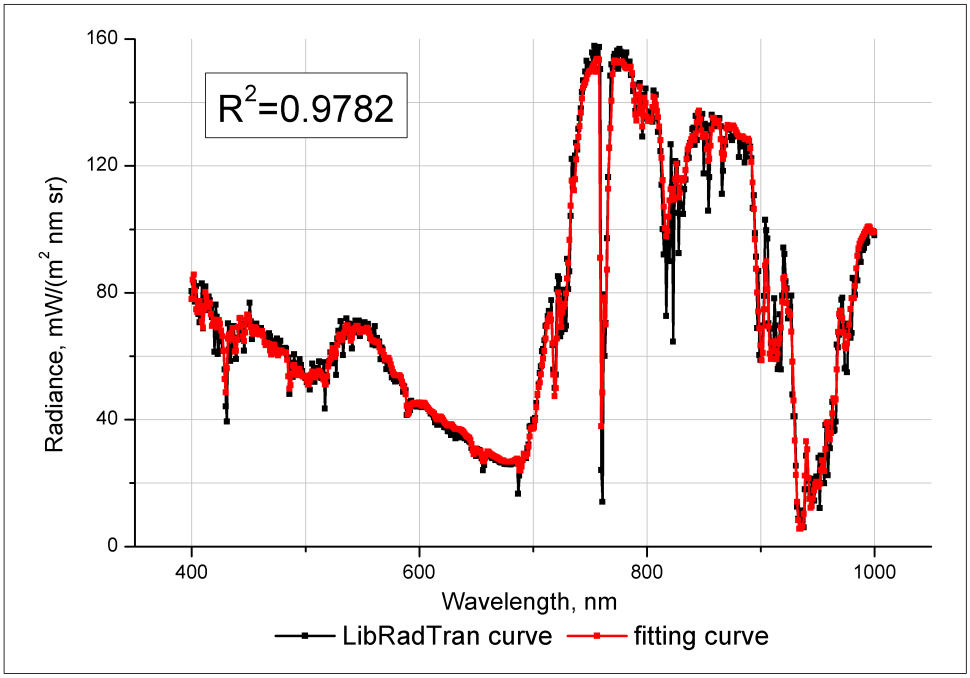

Figure 2. Spectral radiance on TOA according to LibRadTran calculations and fitting an analytic function (21)

The reconstruction accuracy of the spectral reflectance function of the surface (inverse task) is shown in Figs. 3a - 3d, where we present the surface reflectance spectra for four different types of underlying surfaces (water, soil, grass, snow) obtained by SHARC technique using numerically calculated (LibRadTran) TOA brightness spectra, in comparison with the true reflectance data given input for LibRadTran. Fig. 3 reflects the typical retrieved reflectance spectra errors obtained for different types of underlying surfaces.

5.2. Validation using Hyperion measurements

In addition, atmospheric correction of hyperspectral satellite images obtained using the Hyperion sensor on the Earth Observer-1 (EO-1) was performed by us. Three different images with different types of surface were selected, including various types of underlying surfaces such as water, sand, green vegetation, rocks, etc., see in Fig. 4.

Results of the SHARC method were compared with atmospheric correction data of these images in the well-known FLAASH module, implemented in ENVI software package. Typical comparison results for images of Hyperion sensor are shown in Figs. 5, 6, 7. In the left hand side of figures the pixel brightness spectra in absolute units (after radiometric correction) registered by the sensor are shown. The right hand side contains the surface reflectance spectra retrieved by SHARC method and FLAASH module.

It should be noted that the retrieved profiles of SHARC and FLAASH reflectances are in satisfactory agreement. In this case, the SHARC curve is smoother in comparison with FLAASH and shows somewhat better (smoother) behavior in the region of the absorption bands of water vapor around 940 *nm*. We see the "smoothness" of the spectral reflectance reconstructed by the SHARC method (both in the calculated spectra of LibRadTran and in Hyperion satellite spectrum images) in the absorption of water vapor bands. Also one observes that FLAASH often gives negative reflectance values at some spectral ranges (Figs. 6 and 7).

Preprints (www.preprints.org) | NOT PEER-REVIEWED | Posted: 23 October 2018 doi:10.20944/preprints201809.0119.v3

Peer-reviewed version available at Remote Sens. 2018, 10, 1698; doi:10.3390/rs10111698

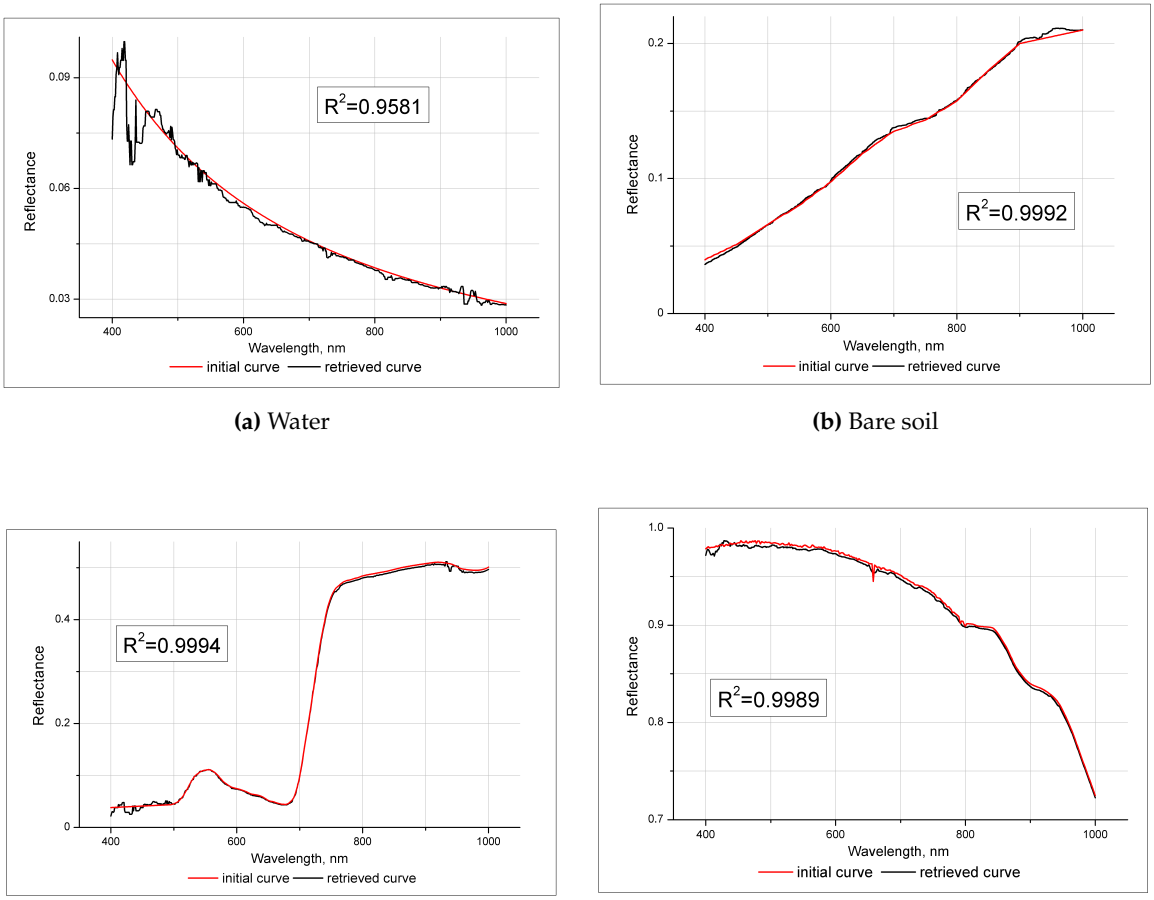

(a) Water **(b)** Bare soil

(c) Grass **(d)** Snow

Figure 3. Surface reflectances for four different surface types (water 3a, bare soil 3b, grass 3c and snow 3d) retrieved by SHARC technique using the numerically calculated (LibRadTran) outgoing TOA radiance spectra, compared to the surface reflectance spectra, initially given in direct problem.

In some cases, the Hyperion sensor gives insufficient quality, as shown, in Fig. 7 for the underlying water surface, where the original spectrum contains "emission bands" around 900 *nm*, which are most probably artifact.

5.3. Validation using ground data

Moreover, to validate our data obtained by the SHARC method, a comparative analysis with ground-based measurements of Radiometric Calibration Network (RadCalNet) was carried out. RadCalNet is an initiative of the Working Group on Calibration and Validation of the Committee on Earth Observation Satellites [23]. This portal provides an open access bottom-of-atmosphere (BOA) and TOA reflectance data measured derived over the network of sites. The data continuously updated, have a 10 nm spectral sampling interval in the spectral range from 380 *nm* to 2500 *nm*.

The Hyperion image that covers of the La Crau site with location in the south of France (43.55N 4.85W) was used. This site area has a thin pebbly soil with sparse vegetation cover [24]. Figure 8 shows the Hyperion image footprint (red rectangle) with location near La Crau (yellow mark). The Hyperion image was acquired on 29.10.2016, 7:48:20 UTC (sun elevation angle: 14.6 deg). RadCalNet data were measured on 29.10.2016, 9:00 UTC (sun elevation angle: 24.11 deg). The results of *in-situ* measured surface reflectance, that corresponds to the pixel number (1719, 476) of Hyperion image mentioned above, were compared with surface reflectance retrieved by SHARC method for this pixel, as shown

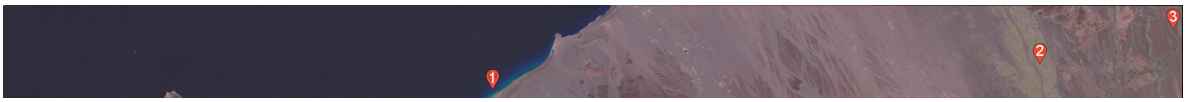

(a) Image was acquired on 17.04.2002 (sun elevation angle: 63.1 deg) and covers territory of south part of Arabian Peninsula (12.96433N 43.42845E)

(b) Image was acquired on 23.08.2007 (sun elevation angle: 55.46 deg) and covers territory of California (Lake Tahoe, 38.86396N 120.01512W)

(c) Image was acquired on 25.10.2014 (sun elevation angle: 34.78 deg) and covers territory near city of Haifa, Israel (32.82167N 35.09679E)

Figure 4. RGB images of the Hyperion based on retrieved spectral surface reflectance functions using the SHARC method.

on Figure 9. A good correspondence of both spectra is found (except vicinity of 450 nm, where there is a slight difference in spectra).

6. Conclusions

A new algorithm for atmospheric correction of hyperspectral images SHARC is presented. This algorithm enables the determination of reflectance of the underlying surface "on the fly" without using a priori information about the atmosphere and the surface. Also we do not use LUTs or time consuming numerical solutions of the radiative transfer equation. Instead the algorithm uses a parameterized analytical solution of the radiative transfer equation for TOA outgoing radiation for a wide range of atmospheric parameters. The type of atmospheric aerosol is not predetermined depending on the season and geographical location, but it is characterized by four unknown parameters accounting for almost all possible types of aerosols.

The advantage of the proposed method is a high accuracy combined with a very short time of performing the procedure of atmospheric correction even for very large images. It takes, for example, for the hypercube with dimension 1546 over 592 pixels and 68 spectral channels, about 15 seconds, on a modern personal computer of standard configuration, with a good accuracy of the spectral reflectance retrieval. The limitation of this method is the above-mentioned range of atmospheric parameters, for which approximations of the functions have been obtained: $g_{\mathbf{a}} \in [0-0.9]$, $\tau \in [0-2]$, $\mu \in [0.2-1.0]$, which, however, covers most realizations of the cloudless atmosphere. Another limitation is the assumption of a horizontal homogeneity of the atmosphere within the image, since the parameters of the atmosphere are assumed to be the same for all pixels. If this assumption is not fulfilled (for example, for large images), the proposed correction method can be applied successively to image subsets (for example, using a sliding rectangular window) and within which the independent parameters of the atmosphere can be obtained. We plan to further develop the method, taking into account the possible horizontal inhomogeneity of the atmosphere, as well as the non-flat terrain.

References

1. Eismann M. Hyperspectral Remote Sensing. Editor, Press., 2012; pp. 725.
2. Miller C. J. Performance assessment of ACORN atmospheric correction algorithm. *Algorithms and Technologies for Multispectral, Hyperspectral, and Ultraspectral Imagery VIII, SPIE* **2002**, *4725*, 438-449.
3. Richter R.; Schlapfer D. Geo-atmospheric processing of airborne imaging spectrometry data. Part 2: Atmospheric/topographic correction. *Int. J. of Remote Sensing* **2002**, *23*, 2631-2649.
4. Gao B.-C.; Heidebrecht K. B.; Goetz A. F. H. Derivation of scaled surface reflectances from AVIRIS data. *Remote Sensing of Environment* **1993**, *44*, 165-178.
5. Adler-Golden S. M.; Matthew M. W.; Bernstein L. S.; Levine R. Y.; Berk A.; Richtsmeier S. C.; Acharya P. K.; Anderson G. P.; Feldeb G.; Gardner J.; Hokeb M.; Jeong L. S.; Pukall B.; Mello J.; Ratkowski A.; Burke H.H. Atmospheric correction for short-wave spectral imagery based on MODTRAN4. *Imaging Spectrometry V, Denver. CO. SPIE* **1999**, *3753*, 61-69.
6. Goetz A. F. H.; Kindel B. C.; Ferri M.; Qu Z. HATCH: Results from simulated radiance, AVIRIS and Hyperion. *JIEEE Transactions on Geoscience and Remote Sensing* **2003**, *6(41)*, 1215-1222.
7. Qu Z.; Kindel B. C.; Goetz A. F. H. The high accuracy atmospheric correction for hyperspectral data (HATCH) model. *IEEE Transactions on Geoscience and Remote Sensing* **2003**, *6(41)*, 1223-1231.
8. Montes M. J.; Gao B.-C.; Davis C. O. Tafkaa atmospheric correction of hyperspectral data. *Imaging Spectrometry IX, SPIE* **2003**, *5159*, 188-197.
9. Leprieur C.; Carrere V.; Gu X. F. Atmospheric corrections and ground reflectance recovery for Airborne Visible/Infrared Imaging Spectrometer (AVIRIS) data: MAC Europe'91. *Photogrammetric Engineering and Remote Sensing* **1995**, *61(10)*, 1233-1238.
10. Katsev I. L.; Prikhach A. S.; Zege E. P.; Grudo J. O.; Kokhanovsky A. A. Speeding up the aerosol optical thickness retrieval using analytical solutions of radiative transfer theory. *Atmos. Meas. Tech.* **2010**, *3*, 1403–1422.
11. Katkovskii L.V. The parameterization of the outgoing radiation for rapid atmospheric correction of hyperspectral images. *Optika atmosfery i okeana.* **2016**, *29(9)*, 778-784.
12. Ginzburg A.S.; Romanov S.V.; Fomin B.A. The radiation-convective model use to estimate the temperature of greenhouse gas potential. *Izvestiya RAN. Fizika atmosfery i okeana.* **2008**, *44(3)*, 324-331.
13. Belyaev B.I.; Belyaev M. Yu.; Desinov L. V.; Katkovsky L.V.; Sarmin E. E. Spectral and Images Processing from Photospectral System in Space Experiment "HURRICANE" on the ISS. *Issledovanie zemli iz kosmosa.* **2014**, *6*, 54–65.
14. Bucholtz A. Rayleigh-scattering calculations for the terrestrial atmosphere. *Applied Optics* **1995**, *34(15)*, 2765-2773.
15. Bassani C., Cavalli R. M., and Antonelli P. Influence of aerosol and surface reflectance variability on hyperspectral observed radiance. *Atmos. Meas. Tech.* **2012**, *5*, 1193–1203.
16. Middleton, W. E. K. Vision through the Atmosphere, University of Toronto Press, Toronto, (1952).
17. Schlapfer D., Borel C. C., Keller J.,and Itten K. I. Atmospheric Precorrected Differential Absorption Technique to Retrieve Columnar Water Vapor. *Remote Sensing of Environment* **1998**, *65*, 353–366.
18. Vasil'ev A.V.; Kuznetsov A.D.; Mel'nikova. I.N. Remote sensing of the environment from space: practice. Editor, Balt.State Tech.University, St.-Petersburg; 2008; pp. 33.
19. Minin I.N. Approximate equations for short-wave radiation absorption calculations in cloudless atmosphere. *Izv. AN SSSR. Fiz. atm. i okeana.* **1984**, *20(10)*, 999-1001.
20. Kokhanovsky A.A.; Mayer B.; Rozanov V.V. A parameterization of the diffuse transmittance and reflectance for aerosol remote sensing problems. *Atmos. Research* **2005**, *73*, 37–43.
21. Vasil'ev A.V.; Kuznetsov A.D.; Mel'nikova. I.N. Approximation of multiply scattered solar radiation in the assumption of single scattering. International Symposium "Atmospheric Radiation and Dynamics" (ISARD 2015); Saint-Petersburg- Petrodvorets, 23 – 26 June 2015; 2015; pp. 131
22. C. Emde, R. Buras-Schnell, A. Kylling, B. Mayer, J. Gasteiger, U. Hamann, J. Kylling, B. Richter, C. Pause, T. Dowling, and L. Bugliaro. The libradtran software package for radiative transfer calculations (version 2.0.1). *Model Development*, **2016**, *9(5)*, 1647-1672.
23. https://www.radcalnet.org/
24. RadCalNet site description CEOS Reference: $QA4EO - WGCV - IVO - CSP - 002\_LC1$, 05 April **2018**, p.5

Preprints (www.preprints.org) | NOT PEER-REVIEWED | Posted: 23 October 2018 doi:10.20944/preprints201809.0119.v3

Peer-reviewed version available at Remote Sens. 2018, 10, 1698; doi:10.3390/rs10111698

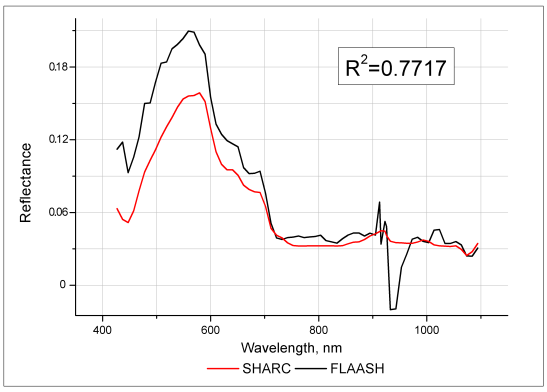

(a) Coastal Water; label#1 in Figure 4a

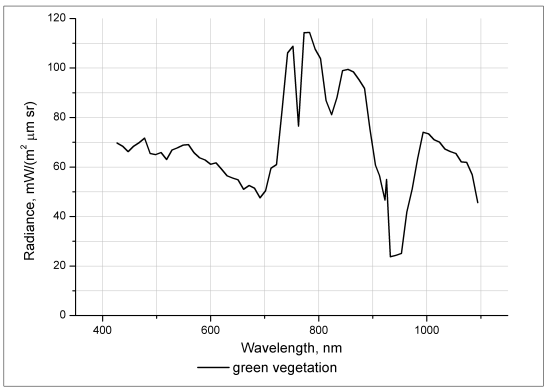

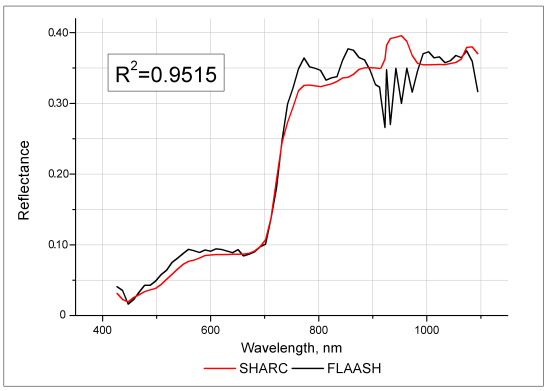

(b) Green Vegetation; label#2 in Figure 4a

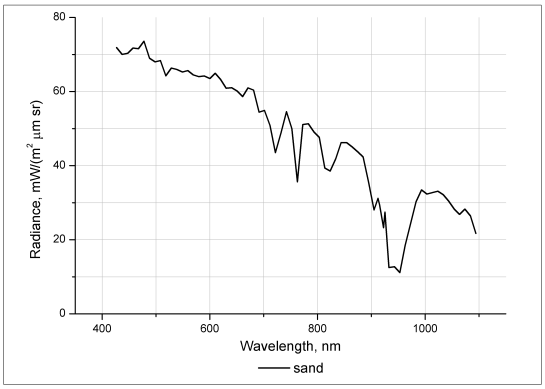

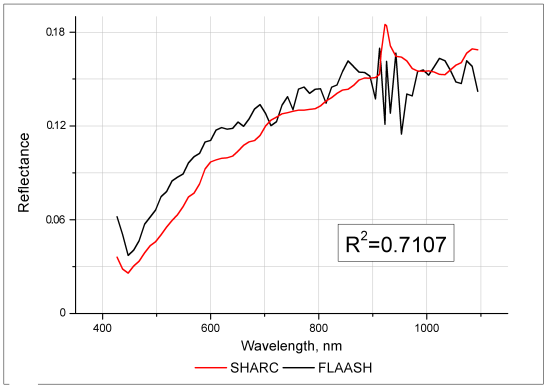

(c) Sand; label#3 in Figure 4a

Figure 5. Initial radiance spectra of Hyperion (left column) and reflectance spectra for the same pixel retrieved by the SHARC atmospheric correction technique (right column) and FLAASH module (ENVI) (right column) for three types of underlying surfaces (coastal water 5a, green vegetation 5b, sand 5c), labeled with pins in Figure 4a.

Preprints (www.preprints.org) | NOT PEER-REVIEWED | Posted: 23 October 2018 doi:10.20944/preprints201809.0119.v3

Peer-reviewed version available at Remote Sens. 2018, 10, 1698; doi:10.3390/rs10111698

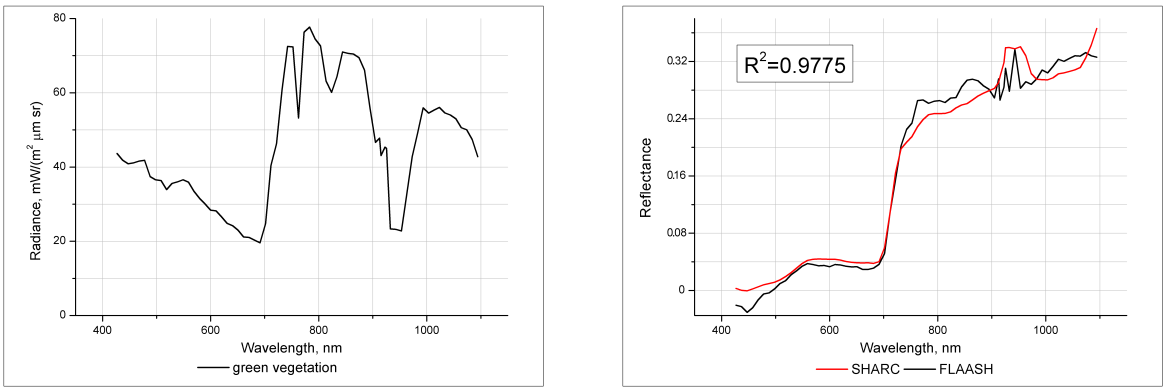

(a) Green Vegetation; label#1 in Figure 4b

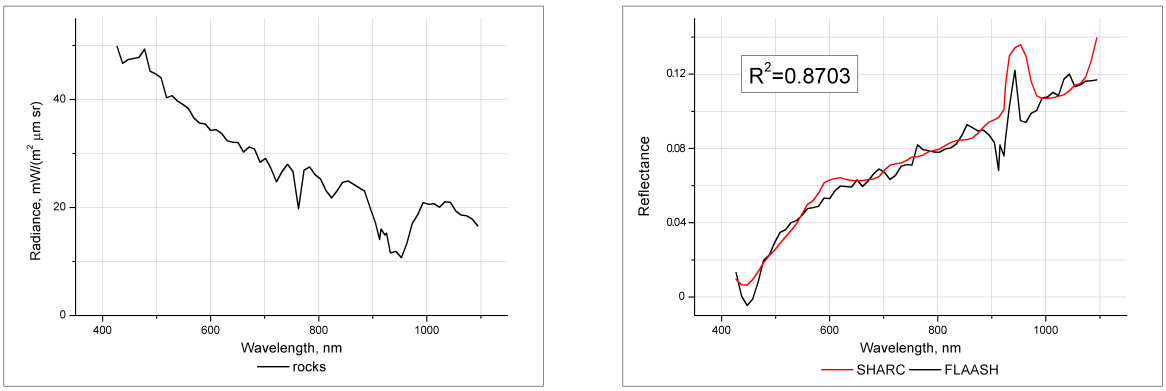

(b) Rocks; label#2 in Figure 4b

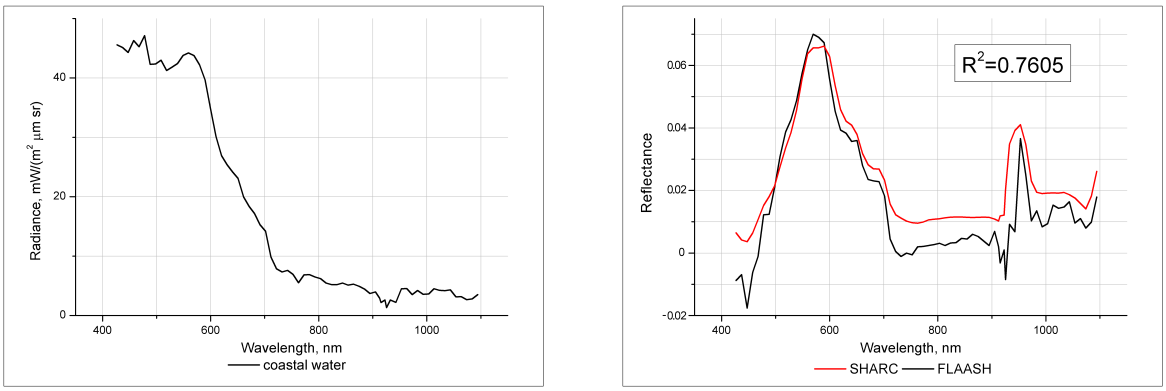

(c) Coastal Water; label#3 in Figure 4b

Figure 6. Initial radiance spectra of Hyperion (left column) and reflectance spectra for the same pixel retrieved by the SHARC atmospheric correction technique (right column) and FLAASH module (ENVI) (right column) for three types of underlying surfaces (green vegetation 6a, rocks 6b, coastal water 6c), labeled with pins in Figure 4b.

Preprints (www.preprints.org) | NOT PEER-REVIEWED | Posted: 23 October 2018 doi:10.20944/preprints201809.0119.v3

Peer-reviewed version available at Remote Sens. 2018, 10, 1698; doi:10.3390/rs10111698

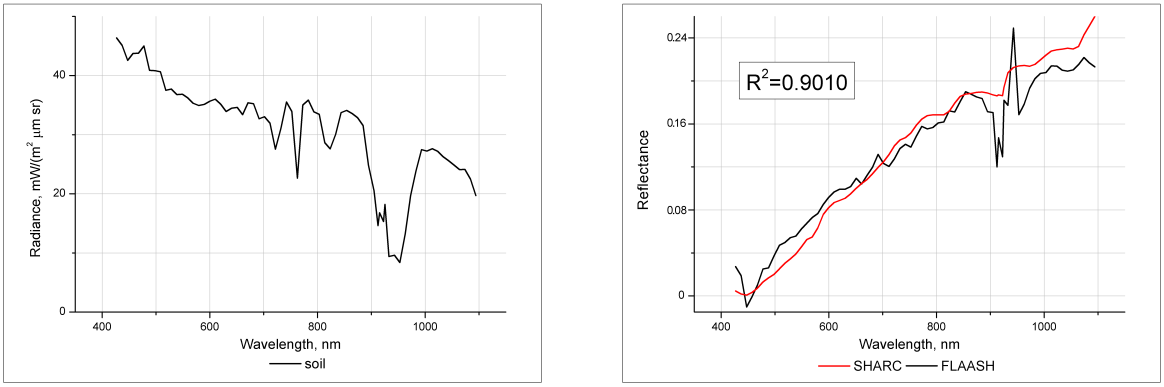

(a) Soil; label#1 in Figure 4c

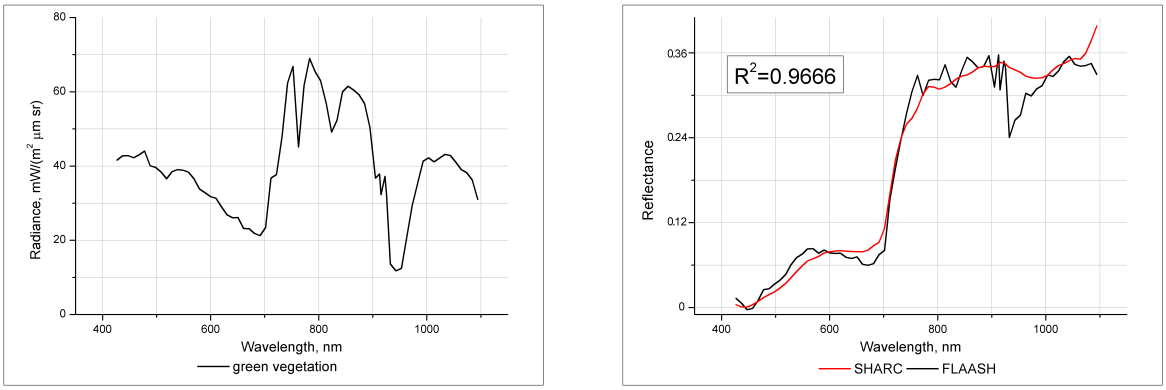

(b) Green Vegetation; label#2 in Figure 4c

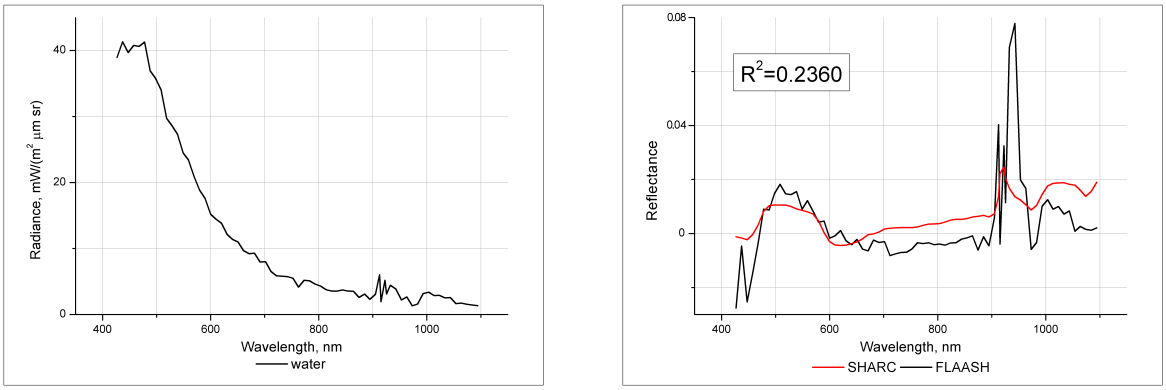

(c) Water; label#3 in Figure 4c

Figure 7. Initial radiance spectra of Hyperion (left column) and reflectance spectra for the same pixel retrieved by the SHARC atmospheric correction technique (right column) and FLAASH module (ENVI) (right column) for three types of underlying surfaces (soil 7a, green vegetation 7b, water 7c), labeled with pins in Figure 4c.

Preprints (www.preprints.org) | NOT PEER-REVIEWED | Posted: 23 October 2018 doi:10.20944/preprints201809.0119.v3

Peer-reviewed version available at Remote Sens. 2018, 10, 1698; doi:10.3390/rs10111698

Figure 8. La Crau site with Hyperion image footprint.

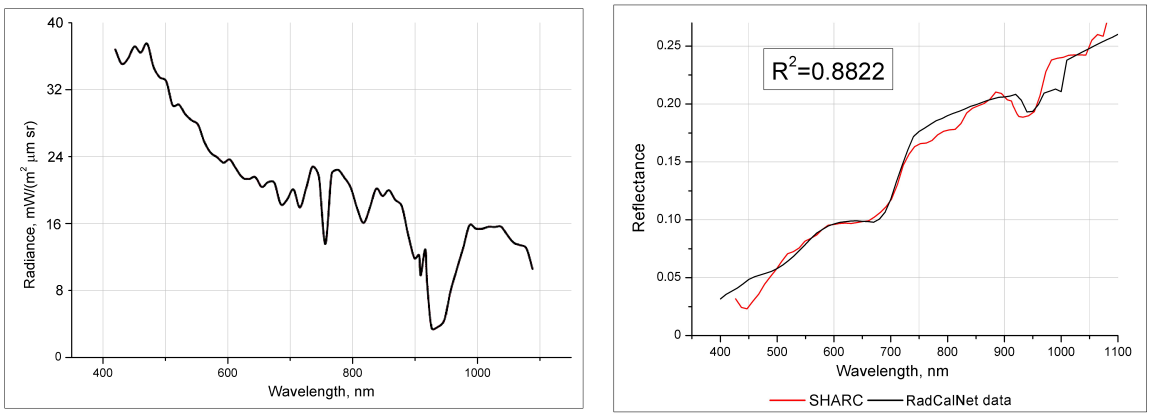

Figure 9. Hyperion radiance spectrum (left side) and measured reflectance of RadCalNet network in compare with calculated reflectance by SHARC method (right side) for the pixel shown on Figure 8.